

Video Deblurring by Fitting to Test Data

Xuanchi Ren* Zian Qian* Qifeng Chen
The Hong Kong University of Science and Technology

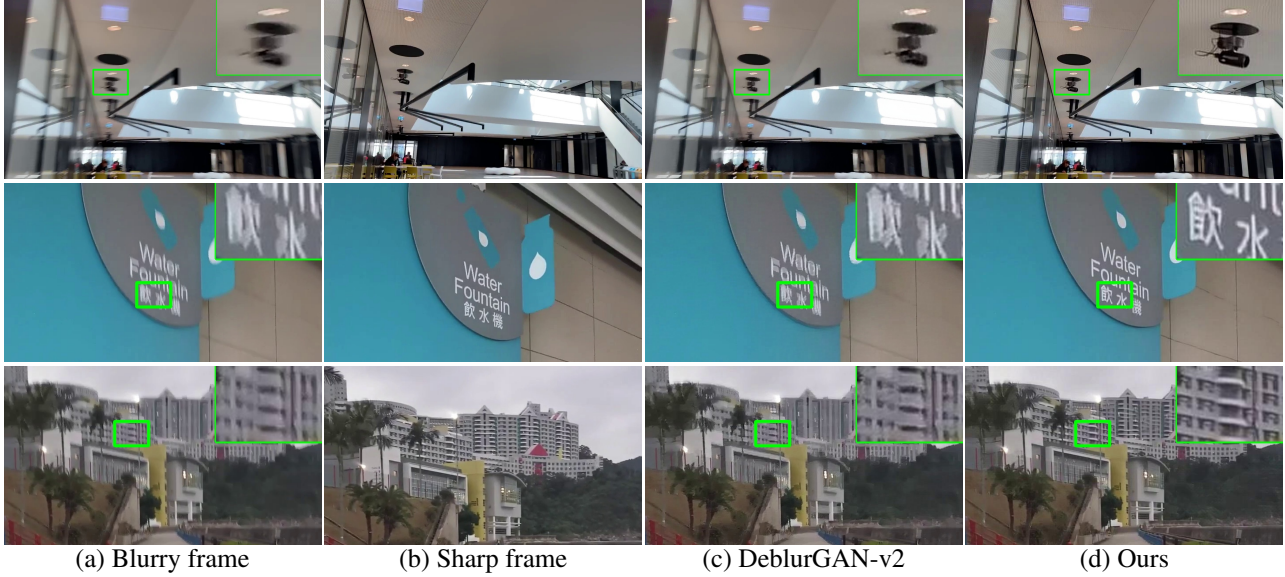


Figure 1: (a) and (b) are two frames from the same video. Note that the sharp textures in (b) can be used to refine (a). (c) is the video deblurring result by a state-of-the-art deblurring method proposed by Kupyn et al. [15] and (d) is our result.

Abstract

We present a novel approach to video deblurring by fitting a deep network to the test video. One key observation is that some frames in a video with motion blur are much sharper than others, and thus we can transfer the texture information in those sharp frames to blurry frames. Our approach heuristically selects sharp frames from a video and then trains a convolutional neural network on these sharp frames. The trained network often absorbs enough details in the scene to perform deblurring on all the video frames. As an internal learning method, our approach has no domain gap between training and test data, which is a problematic issue for existing video deblurring approaches. The conducted experiments on real-world video data show that our model can reconstruct clearer and sharper videos than state-of-the-art video deblurring approaches. Code and data are available at <https://github.com/xrenaa/Deblur-by-Fitting>.

1. Introduction

Video deblurring is a task to recover sharp videos with high fidelity from daily videos with motion blur. A video captured by a handheld smartphone or a moving camera often contains undesirable motion blur in some frames of the video. In practice, users may apply video deblurring techniques to make the video sharper so that the fine details in each frame can be recovered. For instance, a dashcam video may contain critical information about a car plate in some frames that appear to be blurry, and a user would want to recover the underlying details.

Recovering sharp frames from a blurry video is still challenging for learning-based methods due to the domain gap between training and testing data. For example, a model trained on a dataset captured in a library may have bad performance when tested on daily videos captured in a supermarket. Moreover, since it is hard to capture the corresponding sharp and blurry real-world videos, researchers synthesize blurry videos by averaging sharp videos at a high frame rate. As illustrated in Figure 1 (c), the model trained on synthetic data in a different scenario fails to handle the

*Joint first authors

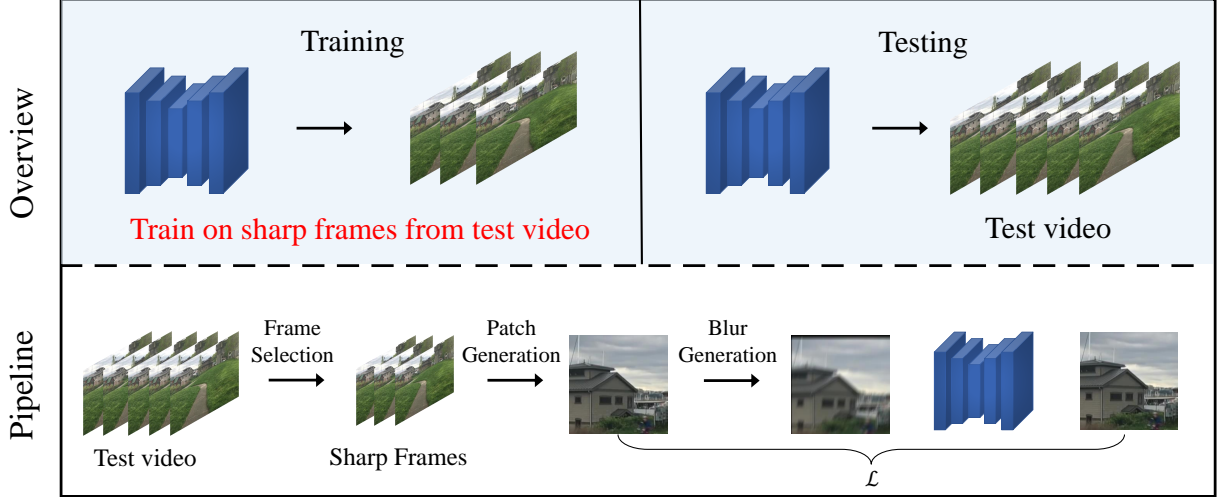


Figure 2: Overview of our fitting-to-test-data pipeline. In our pipeline, for each test video, we fit a deep learning model to it and obtain a test-data-aware model.

motion blur in a real-world video in daily life. Therefore, the state-of-the-art video deblurring methods often produce poor results on real-scene videos.

Researchers have proposed various ideas to address the domain gap issue for video deblurring, but their actual performance is still not satisfactory yet. Kupyn et al. [14, 15] improved the generalization ability of the pre-trained model by estimating the residual between blurry and clear frames. As illustrated in Figure 1, the results are still far from perfect in general scenes. Ulyanov et al. [33] demonstrated that high-frequency information was generated in the posterior phase of the training process. This property forms the basis of internal learning for video deblurring. Ren et al. [23] and Asim et al. [2] estimated blur kernels frame by frame with deep image prior [33]. While these approaches precluded the problem of the domain gap, they still relied on hand-crafted prior and had poor performance on real-world blur, as shown in Figure 3.

To further address the domain gap problem, we introduce a self-supervised pipeline by fitting a deep learning model only on the test video. As shown in Figure 2, unlike traditional supervised pipeline, our method does not rely on training on a large (synthetic) dataset. Our approach is built upon an observation that some frames in a video with motion blur are extremely sharp and clear, as illustrated in Figure 1. Based on this crucial observation, we exploit the internal information of a video by training a simple but efficient convolutional network (CNN) on the sharp-blurry patch pairs generated by our blur generation strategy. As such, our test-data-aware CNN model can adapt to any scenarios and settings of daily videos without the domain gap between training and test data. We also improve our training process with better initialization using MAML [9],

which successfully reduces the running time for a video from hours to 5 minutes.

To analyze the performance of our method, we conduct an extensive user study on Amazon Mechanical Turk. We compare our method with several state-of-the-art image and video deblurring approaches on a real-world dataset, and the result shows our method significantly outperforms the three approaches. Moreover, our accelerated version also achieves state-of-the-art performance in video deblurring while its running time is substantially reduced by two orders of magnitude.

In summary, the contributions of our work are:

- We propose a video deblurring pipeline without the need for a large training dataset by fitting a deep network to the sharp frames in a test video.
- With our blur generation strategy and loss reweighting trick, our pipeline significantly outperforms existing state-of-the-art video deblurring methods, as demonstrated in the user study.
- Combined with meta-learning, our pipeline can be accelerated by about two orders of magnitudes, with little sacrifice in video deblurring quality, but also achieves state-of-the-art performance.
- We collected a dataset containing 70 real-world videos with motion blur that can be used for evaluation on the deblurring task and will be made available to the public.

2. Related Work

Blind deblurring. Early work on image deblurring is often based on manually designed prior by jointly estimated a

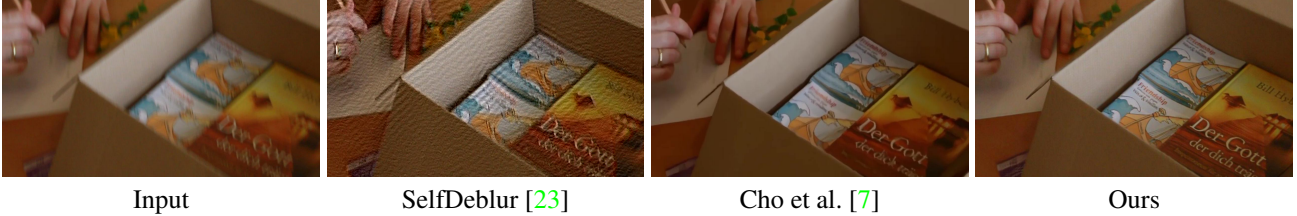


Figure 3: The visual comparison between ours and two internal deblurring methods. The result of Cho et al. [7] is extracted from their demo video. A slight shift is caused by their stabilization. Zoom in for details.

blur kernel and the underlying sharp image via deconvolution [13, 12, 5]. Meanwhile, classic work on video blurring proposed to aggregate neighboring frames and transferred the sharp pixels to the central frames [7]. However, such a traditional method can not handle large depth variations.

Recently, the development of deep learning brings breakthrough to image deblurring task [14, 20, 22, 32, 38]. Nah et al. [20] used an end-to-end multi-scale CNN to restore the images. Kupyn et al. [15] extended the GAN-based method from [14] to Feature Pyramid Network with double-scale discriminator. Lately, Purohit et al. [22] combined attention modules to discover the non-local spatial relationships inside an image for deblurring.

Based on these image deblurring methods, video deblurring benefits from adjacent frames. Su et al. [29] proposed to align the neighbor frames by homograph or optical flow and use a stack of warped frames as input to transfer the image deblurring method to video task. Instead of directly aligning the stack of frames, [34, 42, 43] tried to align the frames in feature space utilizing attention mechanisms. Liu et al. [18] relied on optical flow for a self-supervised pipeline with additional camera parameters.

Blur generation. Obtaining corresponding pairs of sharp and blurred images is of great value for deep learning-based deblurring. The most common approach to blur simulation is to use the average of stacks of sharp frames from video shot by high frame-rate camera [19, 20, 31]. Based on this approach, Brooks et al. [4] proposed a method to apply frame interpolation techniques on a pair of sharp images to produce an abundance of data. These approaches required external reference other than a single image, and the blur synthesized from specific sharp images was fixed. An alternative approach is to convolve the images by “camera shake” kernels. Sun et al. [31] used one out of 73 possible linear motion kernels, and Xu et al. [35] also used linear motion kernels. Recently, Kupyn et al. [14] applied the Markov process to generate trajectories, which were interpolated to form kernels.

Internal learning. Recently, researchers are interested in internal learning instead of learning on a big dataset. Ulyanov et al. [33] showed that the structure of a generator network is capable of capturing image statistics prior to

any learning. Shocher et al. [27] exploited the internal information inside a single image for super-resolution.

Inspired by these works, the concept of internal learning is widely applicable to many tasks. [25, 26] proposed a GAN-based framework to capture the internal distribution of patches within a single image, which could be used in a wide range of image manipulation tasks. To complete blind image deblurring, [2, 23] modified the vanilla DIP [33] work to capture the statics of the clear image and the blur kernel at the same time. Furthermore, for the tasks of video, Zhang et al. [37] proposed an approach built upon DIP [33] and optical flow [30] to conduct video inpainting.

3. Method

3.1. Overview

In the traditional learning-based video deblurring pipeline, the model is first trained on a large-scale dataset for a long time and converges to a single pre-trained model. Then the pre-trained model is used on test data to infer the result. However, this kind of pipeline usually involves a very complex model and cannot solve the domain gap problem between training dataset and test data. For example, a pre-trained model trained in scenario A with high performance usually performs worse on a different scenario B. Kupyn et al. [15] reduce the domain gap by estimating the residual between blur and clear image. Although they successfully improved the performance on test data with a different scenario, it still brings some artifacts.

As shown in Figure 2, unlike the traditional pipeline, we propose a simple but efficient pipeline for video deblurring that addresses the domain gap problem. Some recent approaches, such as SinGAN [25] and InGAN [26] demonstrate that the information in a single image is enough to train a model. We also observe that there are always some sharp frames in a video with motion blur, and more analysis will be presented in the supplementary material. Since frames in a short period contain similar texture information, we can use those sharp frames to refine adjacent blurry frames. In this way, we eliminate the use of large training datasets and directly train the network solely on test data. We also noticed that Cho et al. [7] have a similar

observation to us. They use classical methods rather than a learning-based method to refine blurry frames. As shown in Figure 3, our method can generate images with higher quality and fewer artifacts.

Figure 2 illustrates our proposed pipeline. For a test video with motion blur, we firstly select one sharp frame among every 20 frames based on the variance of the Laplacian map. Since we usually have less than ten selected frames, we employ data augmentation on these frames by randomly cropping the chosen frames into 256×256 patches. We did not find rotation or flipping useful in this task because these data augmentation methods create non-realistic texture information that prevents our model from fitting to the selected frames. Taking those patches as ground truth, we randomly select generated blur kernels and make blurry patches fed into the network as input. After fitting, this on-the-fly model will be used to infer each frame of this video.

3.2. Implementation

3.2.1 Frame selection

The variance of the image Laplacian can be considered as the measurement of the degree of blurriness since it is proportional to the sharpness of an image [3]. Given an image I , the variance of image Laplacian is

$$M_{VL} = \sum_{(i,j) \in I} (\Delta I(i,j) - \overline{\Delta I})^2, \quad (1)$$

where ΔI is the image Laplacian obtained by convolving I with the Laplacian mask and $\overline{\Delta I}$ is the mean value of image Laplacian in I .

There is a trade-off between texture information and the complexity of convergence. Increasing the number of chosen frames will bring more texture information but increase the time and difficulty for the network convergence. Thus, we empirically choose the frame with the highest M_{VL} among every 20 frames to ensure the selected frames cover all texture information in the video.

3.2.2 Blur generation

Since sharp images alone are not enough to train a deblurring network, we need to obtain pairs of corresponding sharp and blurred images with a suitable blur generation strategy. There are three major factors we should take into consideration about blur generation.

First, we notice that the motion blur is mainly caused by camera motion in most cases. Though the camera trajectory may be complex for a long period, the blur kernel is approximately linear in a short period. We represent the local blur kernel M of size $p \times p$ by a motion vector $m = (l, o)$, which characterizes the length and orientation of the motion

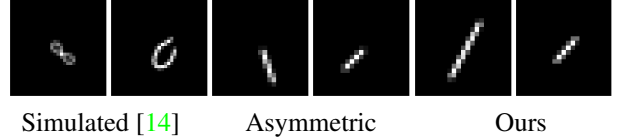


Figure 4: Visualization of three kinds of blur kernels. Our blur kernel is symmetric and linear, which leads to better video deblurred results.

field [31] ($l \in (0, p)$ and $o \in [0, 180^\circ)$). Then the kernel is generated by applying sub-pixel interpolation to the motion vector.

Second, a video frame with motion blur could be considered as the average of a period of time t . We can assume the ground-truth sharp frame is at time $\frac{t}{2}$ for simplicity. Thus we propose to use symmetry blur kernels, which means the center of m is always at the center of the blur kernel M . In Section 4, we empirically show using symmetry blur kernels improves both spatial and temporal stability, compared to simulated blur kernels [14] and asymmetric kernels. Figure 4 visualizes the different kinds of blur kernels.

Third, we consider improving blur generation in the nearly raw data space, rather than the RGB color space. In reality, the motion blur already occurs in raw data before the image signal processing pipeline generates an RGB image. In this way, synthesizing blur in the raw data space is preferred. To simulate the intensity in raw data, we reverse the gamma correction operation. After reversing the gamma correction, the pixel values are roughly linear.

In the end, after selecting sharp patches from patch generation, we perform reversed gamma correction and apply blur kernels to generate patches with motion blur. To reconstruct these images in the RGB space, we apply the gamma correction to them.

3.2.3 Network

In the traditional video deblurring pipeline, the model is trained on an extensive collection of training data with diverse scenarios. To capture different cases, the state-of-the-art models are usually deep with complex components, i.e., deformable convolution [8] and spatial attention, and hence require high computing power and a long period for training. For our pipeline, we found that such deep networks were unnecessary. The performance might even reduce because the small number of training images is not enough for these deep networks. Instead, we find that a simple U-Net [24] is enough to fit our training data well. With our pipeline, the network can aggregate the information in non-local frames instead of several neighboring frames, without the need of optical flow.

3.2.4 Loss function

Rather than using the common pixel-space loss, e.g., the most straightforward L_2 distance, which tends to make the result smooth, we adopt perceptual loss to make a sharp result and preserve more high-frequency information.

Given a trained visual perception network Φ (we use VGG-19 [28]), we define a collection of layers Φ as $\{\Phi_l\}$. For a training pair (I, L) , where L is the ground truth image patch and I is the input image patch, our perceptual loss is

$$\mathcal{L}_P = \sum_l \lambda_l \|\Phi_l(L) - \Phi_l(G(I))\|_1. \quad (2)$$

Here G is the U-Net in our pipeline. The hyperparameters $\{\lambda_l\}$ balance the contribution of each layer l to the loss.

Different from the traditional pipeline, which refers to sharp ground truth images, our method tries to absorb the information of relatively sharp and clear images contained in the test video. Thus, we apply a reweighting strategy to force the network to pay more attention to images of higher sharpness. Note that the variance of image Laplacian M_{VL} used in our pipeline indicates the sharpness of a patch. Thus we normalize the variance by a constant N and multiply it with the original loss function as a reweighted loss function:

$$\mathcal{L}_{reweighted} = \frac{M_{VL}}{N} \mathcal{L}_P. \quad (3)$$

Moreover, to increase the network’s focus on the textural information and further improve the result, we add a Markovian discriminator D that has five hidden layers with WGAN-GP loss [10, 17, 25] to our pipeline.

3.3. Acceleration

Our pipeline exploits the internal information of sharp frames in the test video. However, it usually takes hours to fit a model to these sharp frames for video deblurring due to the complexity and a massive number of possible blur kernels. In our experiments, we notice that the network takes a long period to adapt itself to generate expected sharp images at the beginning of the training. We first used a simple pretraining strategy and found the pretrained model would be easily stuck at a local minimum.

Inspired by [9, 21], we propose to initialize the network via meta-learning, which enables rapid fitting on any given video at test time. We find that model-agnostic meta-learning (MAML) [9] can make the fine-tuning process easier as it provides our model a proper initialization. MAML plays a crucial role in meta-learning due to its high compatibility with various models and tasks by using gradient descent. In our accelerated pipeline, we first initialize our network with ten external test videos (without ground truth) via MAML to lead the model to learn the internal information. At the inference stage, we fine-tune the meta-learned parameters using the given test video in about 5 minutes. The

Algorithm 1 MAML algorithm for deblurring

Require: $p(I)$: Distribution over images

Require: D : a list of blur kernels

Require: α, β : Hyper-parameters (step size)

- 1: Initialize θ
 - 2: **while** not converged **do**
 - 3: Randomly sample a batch of images $\{I_i\} \sim p(I)$ and two blur kernels from D
 - 4: Random crop for image patches $\{GT_i\}$ from $\{I_i\}$
 - 5: Generate $\{Blur_i\}, \{Blur_i^*\}$ from $\{GT_i\}$
 - 6: **for** each i **do**
 - 7: Evaluate $\nabla_{\theta} \mathcal{L}(g_{\theta}(Blur_i), GT_i)$ using \mathcal{L}
 - 8: Compute adapted parameters $\theta_i \leftarrow \theta - \alpha \nabla_{\theta} \mathcal{L}(g_{\theta}(Blur_i), GT_i)$
 - 9: Update $\theta \leftarrow \theta - \beta \nabla_{\theta} \sum_i \mathcal{L}(g_{\theta_i}(Blur_i^*), GT_i)$
-

details of the MAML algorithm for deblurring are shown in Algorithm 1, where $\{I_i\}$ denotes the sharp frames sampled from a small set of test videos, $\{GT_i\}$ denotes the sharp patches cropped from $\{I_i\}$, $\{Blur_i\}$ and $\{Blur_i^*\}$ denote blurry patches generated based on $\{GT_i\}$ using two different blur kernels and g_{θ} denotes our network initialized with the parameter θ .

4. Experiments

4.1. Dataset

In prior video deblurring work, synthetic datasets are often used for evaluation because there are no ground-truth sharp videos for real-world blurry videos. However, we should better evaluate different methods on real-world blurry videos rather than synthetic data. We find that a model training on synthetic data does not necessarily perform well on real-world data. Therefore, we collected a real-world video dataset with 70 videos with motion blur for qualitative and quantitative evaluation. The videos are captured by shaking, walking, or running in diverse indoor and outdoor environments. Each video contains 80-160 frames, shot with iPhone 8 Plus, iPhone 11 Pro Max, or Huawei Mate 20. Although there are no ground-truth sharp videos in our dataset, we can still conduct a user study to compare different methods quantitatively. For the temporal consistency evaluation, we use two synthetic datasets: GOPRO dataset by Su et al. [29] and REDS dataset [19].

4.2. User study

For image restoration tasks like deblurring and super-resolution, PSNR and SSIM are always used to compare among different methods because these metrics are an approximation to human perception of image quality. However, computing PSNR and SSIM is only possible on synthetic data instead of real-world data for video deblurring.

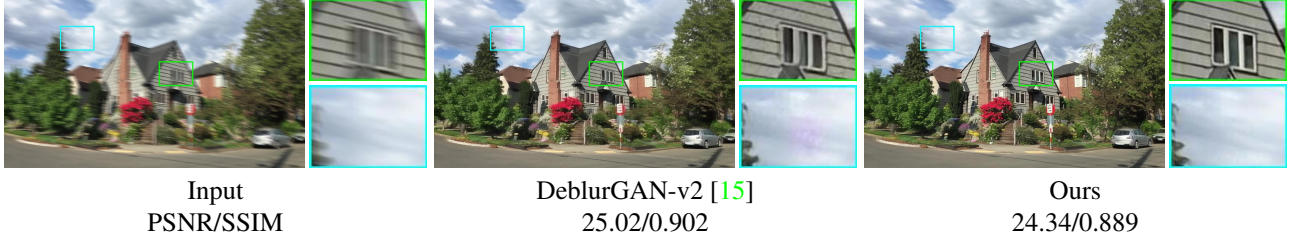


Figure 5: The results on an example in the synthetic dataset. Note that our deblurred result is sharper and clearer than the result by DeblurGAN-v2 [15], but the PSNR and SSIM do not reflect that our result is better.

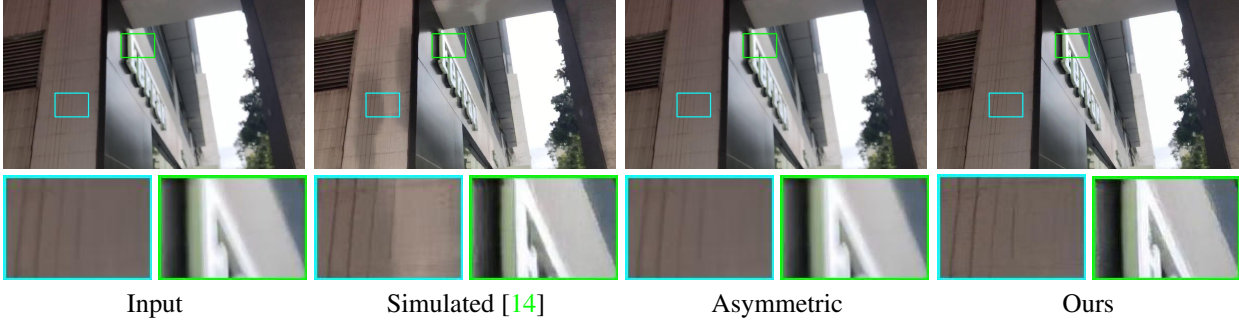


Figure 6: The visual ablation study on different kinds of blur kernels. The symmetric blur kernels improve the spatial stability of our pipeline without bringing artifacts.

Comparison	Ours	Ours-MAML
<i>Image-based methods</i>		
SRN [32]	85.7%	83.7%
Zhang et al. [38]	82.5%	81.9%
DeblurGAN-v2 [15]	80.1%	79.0%
SelfDeblur [23]	93.4%	91.2%
<i>Video-based methods</i>		
EDVR [34]	85.5%	84.7%
DMPHN [36]	94.2%	92.7%
STFAN [43]	79.6%	79.4%

Table 1: User study results of pairwise comparisons of our pipelines and several baselines on the real-world dataset. Each column compares our approach with one of the baselines. Each cell lists the fraction of pairwise comparisons in which images synthesized by our approach were rated more sharper and clearer than images synthesized by the corresponding baseline. Ours-MAML is about two orders of magnitude faster than Ours in terms of speed.

Furthermore, as shown in Figure 5, these metrics may not agree with human perception. Our method is able to recover sharp and clear video frames from a synthetic video, while the result by DeblurGAN-v2 is of lower quality. Therefore, we mainly adopt user study as the main evaluation metric for video deblurring. For the PSNR/SSIM results on syn-

Method	$E_{warp} \downarrow$
DMPHN [36]	0.3155
EDVR [34]	0.2874
STFAN [43]	0.2739
DeblurGAN-v2 [15]	0.2689
Ours (with asymmetric kernels)	0.3274
Ours (with simulated kernels)	0.3928
Ours	0.2599

Table 2: Performance comparison in temporal consistency metric (lower is better). Our method with symmetric kernels achieves the best temporal consistency among all the baselines.

thetic blurry videos, please refer to the supplementary material.

To compare our method with state-of-the-art baselines, we conduct an extensive user study on Amazon Mechanical Turk for both fitting-to-test-data pipeline and accelerated pipeline, following the A/B test protocol proposed by Chen and Koltun [6]. Among all the prior work, we choose several representative blind image and video deblurring methods for comparisons: SRN (CVPR 2018) [32], Zhang et al. (CVPR 2018) [38], DMPHN (CVPR 2019) [36], EDVR (CVPRW 2019) [34], DeblurGAN-v2 (ICCV 2019) [15], STFAN (ICCV 2019) [43], and SelfDeblur

Comparison	Ours
Ours without reweighting	66.0%
Ours without reversed gamma	83.7%
Ours with simulated kernels	61.7%
Ours with asymmetric kernels	84.0%

Table 3: User study results for ablation study, showing the preference rate of our complete model vs. an ablated model. The images attained with reweighting, reversed gamma correction, and symmetric blur kernels are preferred by users.

(CVPR 2020) [23]. For all these baselines, we use their public pre-trained models.

Instead of showing videos, we choose to randomly sample one blurry frame from each video so that participants have more time to focus on the details of the results. The sampled image is cropped into a square of size 720×720 for better judgment. We sample one blurry frame from each video in our real-world dataset for comparisons, which results in a total of 70 comparisons. During the user study, each user is presented with an image deblurred by our method and an image deblurred by a baseline simultaneously in a random order in the same row. Then the user needs to choose an image that is sharper and clearer between the two deblurred images. The results are summarized in Table 1.

According to Table 1, the rates of Ours are all larger than the baselines, which shows our fitting-to-test-data pipeline is preferred by most users. To some extent, our accelerated pipeline sacrifices the image quality to shorten the running time to about 5 minutes. However, it can still outperform the state-of-the-art methods.

All the results are statistically significant with $p < 1 \times 10^{-3}$, and 30 participants are involved in each comparison. Figure 13 displays visual comparison examples on different scenarios. We show more comparisons in the supplementary material.

4.3. Temporal consistency

We evaluate the temporal consistency by estimating the warping error E_{warp} proposed in [16]. We compare the temporal consistency of our method with DMPHN [36], EDVR [34], STFAN [43] and DeblurGAN-v2 [15]. As shown in Table 2, our method have the lowest warping error and thus best temporal consistency, though our method is on image level. For this metric, We random sample 10 videos from the synthetic datasets [19, 29]. Please refer to the supplementary video for further demonstration of the temporal consistency.

Comparison	Our post-processing
EDVR [34]	73.3%
STFAN [43]	86.0%

(a) Results of user study.

Method	Original	Our post-processing
EDVR [34]	0.2779	0.2681
STFAN [43]	0.2716	0.2630

(b) Results of temporal consistency.

Table 4: Comparison between original results by baselines and the post-processing results by our pipeline.

4.4. Ablation study

In addition to the qualitative comparison for blur kernels shown in Figure 6, we also perform an ablation study for different components of our fitting-to-test-data pipeline. As shown in Table 2, we show our proposed symmetric kernels can better improve temporal stability, compared to asymmetric and simulated kernels.

We then show that our reweighting strategy for the loss function, the reverse of gamma correction in blur generation, and symmetric kernels can further improve the performance. We conduct an additional user study on Amazon Mechanical Turk following the above protocol to evaluate the influence brought by these components in our pipeline. As summarized in Table 3, users prefer the results synthesized by the pipeline with our full model. For each comparison, we randomly sample 10 images from our real-world video deblurring dataset, and 15 participants are involved in the user study.

4.5. Extension

In an extreme case, when there are no sharp frames in the test video, our method can also serve as a post-processing step for an existing video deblurring model. We can first apply a pretrained video deblurring model and then use the resulted video as the input to our pipeline for further refinement. We use our pipeline to refine the results by EDVR [34] and STFAN [43] and sample 30 videos from the synthetic datasets for comparison. As shown in Table 4b, the videos become more temporally consistent after our post-processing. The video quality is also enhanced, as demonstrated in Table 4a. The qualitative comparison is shown in Figure 7.

5. Conclusion

We have demonstrated the effectiveness of our fitting-to-test-data pipeline for video deblurring. Our approach avoids the domain gap issue between training and test by



Figure 7: Visual comparison between the results produced by baselines and the post-processing results by our pipeline.

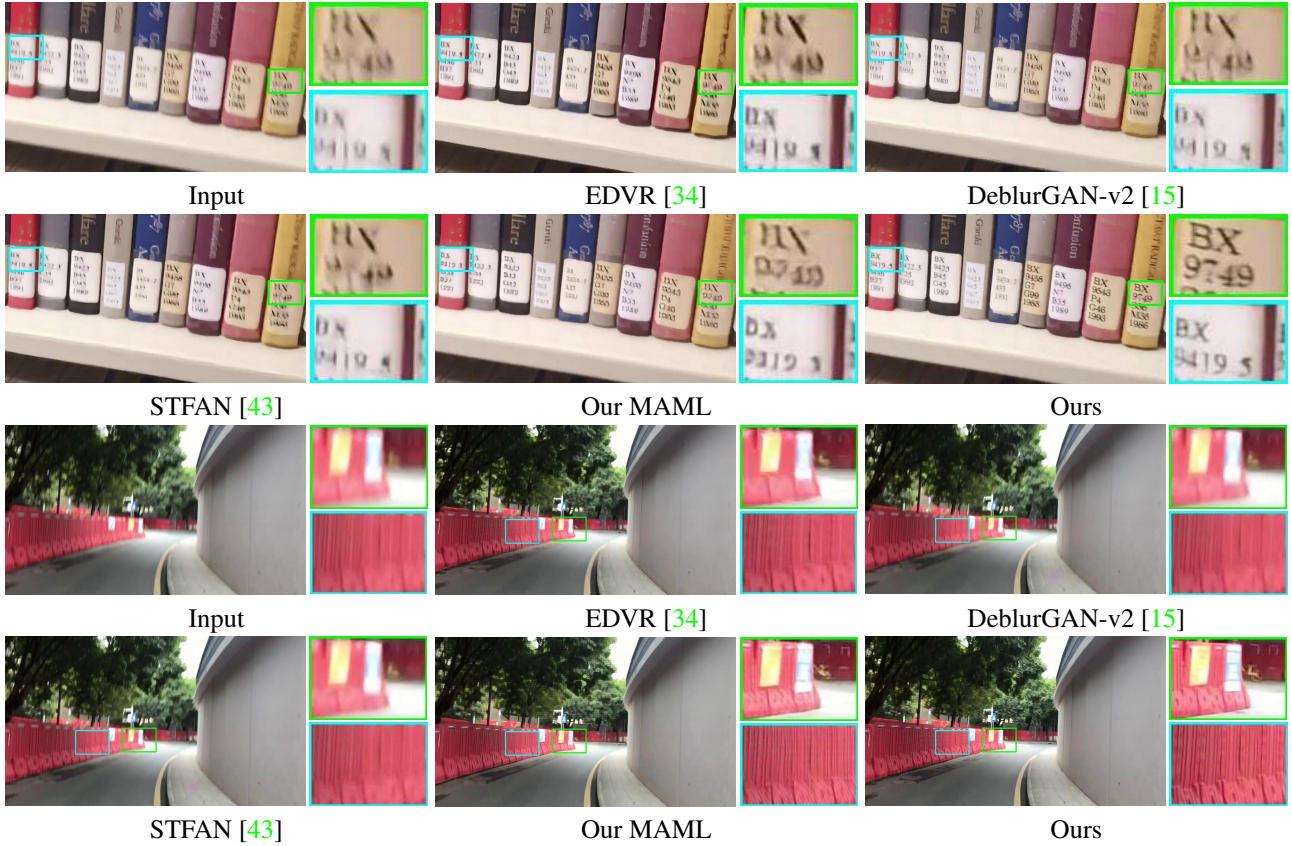


Figure 8: Visual comparisons on our real-world video deblurring dataset. Ours is from our fitting-to-test-data pipeline, and our MAML is from our accelerated pipeline. Our method is capable of restoring the text and high-frequency information.

fitting a deep network on the test video only. Our approach is also based on a key observation that there are almost always sharp frames in a blurry video so that we can train a deep model on those sharper video frames. To evaluate our method and prior work on real-world data for video deblurring, we collected a dataset containing videos with motion blur, and the dataset will be released publicly. Furthermore, we have applied meta-learning to accelerate our

pipeline significantly, while the quality of deblurred videos only degrades a little bit. To further improve our approach in the future, joint learning of realistic blur kernels in our model is a promising direction. We hope our fitting-to-test-data pipeline can inspire more researchers to tackle image and video processing with a new paradigm.

References

- [1] Martín Abadi, Paul Barham, Jianmin Chen, Zhifeng Chen, Andy Davis, Jeffrey Dean, Matthieu Devin, Sanjay Ghemawat, Geoffrey Irving, Michael Isard, et al. Tensorflow: A system for large-scale machine learning. In *OSDI*, 2016. 12
- [2] Muhammad Asim, Fahad Shamshad, and Ali Ahmed. Blind image deconvolution using pretrained generative priors. *arXiv:1908.07404*, 2019. 2, 3
- [3] R. Bansal, G. Raj, and T. Choudhury. Blur image detection using laplacian operator and open-cv. In *SMART*, 2016. 4
- [4] Tim Brooks and Jonathan T Barron. Learning to synthesize motion blur. In *CVPR*, 2019. 3
- [5] Chia-Feng Chang and Jiunn-Lin Wu. A new single image deblurring algorithm using hyper laplacian priors. In *ICS*, 2014. 3
- [6] Qifeng Chen and Vladlen Koltun. Photographic image synthesis with cascaded refinement networks. In *ICCV*, 2017. 6
- [7] Sunghyun Cho, Jue Wang, and Seungyong Lee. Video deblurring for hand-held cameras using patch-based synthesis. *ACM Transactions on Graphics (TOG)*, 2012. 3
- [8] Jifeng Dai, Haozhi Qi, Yuwen Xiong, Yi Li, Guodong Zhang, Han Hu, and Yichen Wei. Deformable convolutional networks. In *ICCV*, 2017. 4
- [9] Chelsea Finn, Pieter Abbeel, and Sergey Levine. Model-agnostic meta-learning for fast adaptation of deep networks. In *ICML*, 2017. 2, 5
- [10] Ishaan Gulrajani, Faruk Ahmed, Martín Arjovsky, Vincent Dumoulin, and Aaron C. Courville. Improved training of wasserstein gans. In *NeurIPS*, 2017. 5
- [11] Diederik P. Kingma and Jimmy Ba. Adam: A method for stochastic optimization. In *ICLR*, 2015. 12
- [12] Dilip Krishnan, Terence Tay, and Rob Fergus. Blind deconvolution using a normalized sparsity measure. In *CVPR*, 2011. 3
- [13] Deepa Kundur and Dimitrios Hatzinakos. Blind image deconvolution. *IEEE signal processing magazine*, 1996. 3
- [14] Orest Kupyn, Volodymyr Budzan, Mykola Mykhailych, Dmytro Mishkin, and Jiri Matas. Deblurgan: Blind motion deblurring using conditional adversarial networks. In *CVPR*, 2018. 2, 3, 4, 6
- [15] Orest Kupyn, Tetiana Martyniuk, Junru Wu, and Zhangyang Wang. Deblurgan-v2: Deblurring (orders-of-magnitude) faster and better. In *ICCV*, 2019. 1, 2, 3, 6, 7, 8, 13, 16, 17, 18, 19, 20, 21
- [16] Chenyang Lei, Yazhou Xing, and Qifeng Chen. Blind video temporal consistency via deep video prior. In *NeurIPS*, 2020. 7
- [17] Chuan Li and Michael Wand. Precomputed real-time texture synthesis with markovian generative adversarial networks. In *ECCV*, 2016. 5
- [18] Peidong Liu, Joel Janai, Marc Pollefeys, Torsten Sattler, and Andreas Geiger. Self-supervised linear motion deblurring. *RA-L*. 3
- [19] Seungjun Nah, Sungyong Baik, Seokil Hong, Gyeongsik Moon, Sanghyun Son, Radu Timofte, and Kyoung Mu Lee. Ntire 2019 challenge on video deblurring and super-resolution: Dataset and study. In *CVPR Workshops*, 2019. 3, 5, 7, 12, 15
- [20] Seungjun Nah, Tae Hyun Kim, and Kyoung Mu Lee. Deep multi-scale convolutional neural network for dynamic scene deblurring. In *CVPR*, 2017. 3, 12
- [21] Seobin Park, Jinsu Yoo, Donghyeon Cho, Jiwon Kim, and Tae Hyun Kim. Fast adaptation to super-resolution networks via meta-learning. *arXiv:2001.02905*, 2020. 5
- [22] Kuldeep Purohit and AN Rajagopalan. Region-adaptive dense network for efficient motion deblurring. In *AAAI*, 2020. 3
- [23] Dongwei Ren, Kai Zhang, Qilong Wang, Qinghua Hu, and Wangmeng Zuo. Neural blind deconvolution using deep priors. In *CVPR*, 2020. 2, 3, 6, 7
- [24] Olaf Ronneberger, Philipp Fischer, and Thomas Brox. U-net: Convolutional networks for biomedical image segmentation. In *MICCAI*, 2015. 4
- [25] Tamar Rott Shaham, Tali Dekel, and Tomer Michaeli. Singan: Learning a generative model from a single natural image. In *ICCV*, 2019. 3, 5
- [26] Assaf Shocher, Shai Bagon, Phillip Isola, and Michal Irani. Ingan: Capturing and remapping the” dna” of a natural image. In *ICCV*, 2019. 3
- [27] Assaf Shocher, Nadav Cohen, and Michal Irani. “zero-shot” super-resolution using deep internal learning. In *CVPR*, 2018. 3
- [28] Karen Simonyan and Andrew Zisserman. Very deep convolutional networks for large-scale image recognition. In *ICLR*, 2015. 5, 12
- [29] Shuochen Su, Mauricio Delbracio, Jue Wang, Guillermo Sapiro, Wolfgang Heidrich, and Oliver Wang. Deep video deblurring for hand-held cameras. In *CVPR*, 2017. 3, 5, 7, 12, 13, 15
- [30] Deqing Sun, Xiaodong Yang, Ming-Yu Liu, and Jan Kautz. Pwc-net: Cnns for optical flow using pyramid, warping, and cost volume. In *CVPR*, 2018. 3
- [31] Jian Sun, Wenfei Cao, Zongben Xu, and Jean Ponce. Learning a convolutional neural network for non-uniform motion blur removal. In *CVPR*, 2015. 3, 4
- [32] Xin Tao, Hongyun Gao, Xiaoyong Shen, Jue Wang, and Ji-aya Jia. Scale-recurrent network for deep image deblurring. In *CVPR*, 2018. 3, 6
- [33] Dmitry Ulyanov, Andrea Vedaldi, and Victor Lempitsky. Deep image prior. In *CVPR*, 2018. 2, 3
- [34] Xintao Wang, Kelvin CK Chan, Ke Yu, Chao Dong, and Chen Change Loy. Edvr: Video restoration with enhanced deformable convolutional networks. In *CVPR Workshops*, 2019. 3, 6, 7, 8, 12, 13, 14, 17, 18, 19, 20, 21
- [35] Li Xu, Jimmy SJ Ren, Ce Liu, and Jiaya Jia. Deep convolutional neural network for image deconvolution. In *NeurIPS*, 2014. 3
- [36] Hongguang Zhang, Yuchao Dai, Hongdong Li, and Piotr Koniusz. Deep stacked hierarchical multi-patch network for image deblurring. In *CVPR*, 2019. 6, 7, 13, 17, 18, 19, 20, 21

- [37] Haotian Zhang, Long Mai, Ning Xu, Zhaowen Wang, John Collomosse, and Hailin Jin. An internal learning approach to video inpainting. In *ICCV*, 2019. 3
- [38] Jiawei Zhang, Jinshan Pan, Jimmy S. J. Ren, Yibing Song, Linchao Bao, Rynson W. H. Lau, and Ming-Hsuan Yang. Dynamic scene deblurring using spatially variant recurrent neural networks. In *CVPR*, 2018. 3, 6
- [39] Richard Zhang, Phillip Isola, Alexei A Efros, Eli Shechtman, and Oliver Wang. The unreasonable effectiveness of deep features as a perceptual metric. In *CVPR*, 2018. 12, 13, 14
- [40] Richard Zhang, Phillip Isola, Alexei A Efros, Eli Shechtman, and Oliver Wang. The unreasonable effectiveness of deep features as a perceptual metric. In *CVPR*, 2018. 13, 14
- [41] Xuaner Zhang, Ren Ng, and Qifeng Chen. Single image reflection separation with perceptual losses. In *CVPR*, 2018. 12
- [42] Shangchen Zhou, Jiawei Zhang, Jinshan Pan, Haozhe Xie, Wangmeng Zuo, and Jimmy Ren. Spatio-temporal filter adaptive network for video deblurring. In *ICCV*, 2019. 3
- [43] Shangchen Zhou, Jiawei Zhang, Jinshan Pan, Haozhe Xie, Wangmeng Zuo, and Jimmy Ren. Spatio-temporal filter adaptive network for video deblurring. In *ICCV*, 2019. 3, 6, 7, 8, 19, 20, 21
- [12] Dilip Krishnan, Terence Tay, and Rob Fergus. Blind deconvolution using a normalized sparsity measure. In *CVPR*, 2011. 3
- [13] Deepa Kundur and Dimitrios Hatzinakos. Blind image deconvolution. *IEEE signal processing magazine*, 1996. 3
- [14] Orest Kupyn, Volodymyr Budzan, Mykola Mykhailych, Dmytro Mishkin, and Jiri Matas. Deblurgan: Blind motion deblurring using conditional adversarial networks. In *CVPR*, 2018. 2, 3, 4, 6
- [15] Orest Kupyn, Tetiana Martyniuk, Junru Wu, and Zhangyang Wang. Deblurgan-v2: Deblurring (orders-of-magnitude) faster and better. In *ICCV*, 2019. 1, 2, 3, 6, 7, 8, 13, 16, 17, 18, 19, 20, 21
- [16] Chenyang Lei, Yazhou Xing, and Qifeng Chen. Blind video temporal consistency via deep video prior. In *NeurIPS*, 2020. 7
- [17] Chuan Li and Michael Wand. Precomputed real-time texture synthesis with markovian generative adversarial networks. In *ECCV*, 2016. 5
- [18] Peidong Liu, Joel Janai, Marc Pollefeys, Torsten Sattler, and Andreas Geiger. Self-supervised linear motion deblurring. *RA-L*. 3
- [19] Seungjun Nah, Sungyong Baik, Seokil Hong, Gyeongsik Moon, Sanghyun Son, Radu Timofte, and Kyoung Mu Lee. Ntire 2019 challenge on video deblurring and super-resolution: Dataset and study. In *CVPR Workshops*, 2019. 3, 5, 7, 12, 15
- [20] Seungjun Nah, Tae Hyun Kim, and Kyoung Mu Lee. Deep multi-scale convolutional neural network for dynamic scene deblurring. In *CVPR*, 2017. 3, 12
- [21] Seobin Park, Jinsu Yoo, Donghyeon Cho, Jiwon Kim, and Tae Hyun Kim. Fast adaptation to super-resolution networks via meta-learning. *arXiv:2001.02905*, 2020. 5
- [22] Kuldeep Purohit and AN Rajagopalan. Region-adaptive dense network for efficient motion deblurring. In *AAAI*, 2020. 3
- [23] Dongwei Ren, Kai Zhang, Qilong Wang, Qinghua Hu, and Wangmeng Zuo. Neural blind deconvolution using deep priors. In *CVPR*, 2020. 2, 3, 6, 7
- [24] Olaf Ronneberger, Philipp Fischer, and Thomas Brox. U-net: Convolutional networks for biomedical image segmentation. In *MICCAI*, 2015. 4
- [25] Tamar Rott Shaham, Tali Dekel, and Tomer Michaeli. Singan: Learning a generative model from a single natural image. In *ICCV*, 2019. 3, 5
- [26] Assaf Shocher, Shai Bagon, Phillip Isola, and Michal Irani. Ingan: Capturing and remapping the “dna” of a natural image. In *ICCV*, 2019. 3
- [27] Assaf Shocher, Nadav Cohen, and Michal Irani. “zero-shot” super-resolution using deep internal learning. In *CVPR*, 2018. 3
- [28] Karen Simonyan and Andrew Zisserman. Very deep convolutional networks for large-scale image recognition. In *ICLR*, 2015. 5, 12
- [29] Shuo Chen Su, Mauricio Delbracio, Jue Wang, Guillermo Sapiro, Wolfgang Heidrich, and Oliver Wang. Deep video deblurring for hand-held cameras. In *CVPR*, 2017. 3, 5, 7, 12, 13, 15

References

- [1] Martín Abadi, Paul Barham, Jianmin Chen, Zhifeng Chen, Andy Davis, Jeffrey Dean, Matthieu Devin, Sanjay Ghemawat, Geoffrey Irving, Michael Isard, et al. Tensorflow: A system for large-scale machine learning. In *OSDI*, 2016. 12
- [2] Muhammad Asim, Fahad Shamshad, and Ali Ahmed. Blind image deconvolution using pretrained generative priors. *arXiv:1908.07404*, 2019. 2, 3
- [3] R. Bansal, G. Raj, and T. Choudhury. Blur image detection using laplacian operator and open-cv. In *SMART*, 2016. 4
- [4] Tim Brooks and Jonathan T Barron. Learning to synthesize motion blur. In *CVPR*, 2019. 3
- [5] Chia-Feng Chang and Jiunn-Lin Wu. A new single image deblurring algorithm using hyper laplacian priors. In *ICS*, 2014. 3
- [6] Qifeng Chen and Vladlen Koltun. Photographic image synthesis with cascaded refinement networks. In *ICCV*, 2017. 6
- [7] Sunghyun Cho, Jue Wang, and Seungyong Lee. Video deblurring for hand-held cameras using patch-based synthesis. *ACM Transactions on Graphics (TOG)*, 2012. 3
- [8] Jifeng Dai, Haozhi Qi, Yuwen Xiong, Yi Li, Guodong Zhang, Han Hu, and Yichen Wei. Deformable convolutional networks. In *ICCV*, 2017. 4
- [9] Chelsea Finn, Pieter Abbeel, and Sergey Levine. Model-agnostic meta-learning for fast adaptation of deep networks. In *ICML*, 2017. 2, 5
- [10] Ishaan Gulrajani, Faruk Ahmed, Martín Arjovsky, Vincent Dumoulin, and Aaron C. Courville. Improved training of wasserstein gans. In *NeurIPS*, 2017. 5
- [11] Diederik P. Kingma and Jimmy Ba. Adam: A method for stochastic optimization. In *ICLR*, 2015. 12

- [30] Deqing Sun, Xiaodong Yang, Ming-Yu Liu, and Jan Kautz. Pwc-net: Cnns for optical flow using pyramid, warping, and cost volume. In *CVPR*, 2018. 3
- [31] Jian Sun, Wenfei Cao, Zongben Xu, and Jean Ponce. Learning a convolutional neural network for non-uniform motion blur removal. In *CVPR*, 2015. 3, 4
- [32] Xin Tao, Hongyun Gao, Xiaoyong Shen, Jue Wang, and Jiaya Jia. Scale-recurrent network for deep image deblurring. In *CVPR*, 2018. 3, 6
- [33] Dmitry Ulyanov, Andrea Vedaldi, and Victor Lempitsky. Deep image prior. In *CVPR*, 2018. 2, 3
- [34] Xintao Wang, Kelvin CK Chan, Ke Yu, Chao Dong, and Chen Change Loy. Edvr: Video restoration with enhanced deformable convolutional networks. In *CVPR Workshops*, 2019. 3, 6, 7, 8, 12, 13, 14, 17, 18, 19, 20, 21
- [35] Li Xu, Jimmy SJ Ren, Ce Liu, and Jiaya Jia. Deep convolutional neural network for image deconvolution. In *NeurIPS*, 2014. 3
- [36] Hongguang Zhang, Yuchao Dai, Hongdong Li, and Piotr Koniusz. Deep stacked hierarchical multi-patch network for image deblurring. In *CVPR*, 2019. 6, 7, 13, 17, 18, 19, 20, 21
- [37] Haotian Zhang, Long Mai, Ning Xu, Zhaowen Wang, John Collomosse, and Hailin Jin. An internal learning approach to video inpainting. In *ICCV*, 2019. 3
- [38] Jiawei Zhang, Jinshan Pan, Jimmy S. J. Ren, Yibing Song, Linchao Bao, Rynson W. H. Lau, and Ming-Hsuan Yang. Dynamic scene deblurring using spatially variant recurrent neural networks. In *CVPR*, 2018. 3, 6
- [39] Richard Zhang, Phillip Isola, Alexei A Efros, Eli Shechtman, and Oliver Wang. The unreasonable effectiveness of deep features as a perceptual metric. In *CVPR*, 2018. 12, 13, 14
- [40] Richard Zhang, Phillip Isola, Alexei A Efros, Eli Shechtman, and Oliver Wang. The unreasonable effectiveness of deep features as a perceptual metric. In *CVPR*, 2018. 13, 14
- [41] Xuaner Zhang, Ren Ng, and Qifeng Chen. Single image reflection separation with perceptual losses. In *CVPR*, 2018. 12
- [42] Shangchen Zhou, Jiawei Zhang, Jinshan Pan, Haozhe Xie, Wangmeng Zuo, and Jimmy Ren. Spatio-temporal filter adaptive network for video deblurring. In *ICCV*, 2019. 3
- [43] Shangchen Zhou, Jiawei Zhang, Jinshan Pan, Haozhe Xie, Wangmeng Zuo, and Jimmy Ren. Spatio-temporal filter adaptive network for video deblurring. In *ICCV*, 2019. 3, 6, 7, 8, 19, 20, 21

A. Implementation details

All the models are implemented in Tensorflow [1] and trained on Nvidia GeForce GTX 1080 Ti GPUs. For our fitting-to-test-data pipeline trained from scratch, it takes 8 hours to train the models for 400,000 iterations. For the loss function, the hyper-parameters $\{\lambda_l\}$ are adopted from Zhang et al. [41] and the constant $N = 100$. We used Adam [11] for all the networks with a learning rate of 5×10^{-5} for the U-Net and 1×10^{-4} for the Markovian Discriminator. For our accelerate pipeline, the model takes approximately 5 minutes to refine for 4000 iterations. In the MAML algorithm, α is set to be 1×10^{-4} and β is set to be 1×10^{-5} . The hyper-parameters for the loss function remains the same. For the layers $\{\Phi_l\}$, we use ‘conv1_2’, ‘conv2_2’, ‘conv3_2’, ‘conv4_2’, and ‘conv5_2’ in VGG-19 [28].

Moreover, for the details of the blur kernel dictionary, we have 2000 blur kernels of size 21×21 , 4000 blur kernels of size 31×31 , and 2000 blur kernels of size 41×41 . In the procedure of generation, we random a pair (l, o) and generate two blur kernels based on $m = (l, o)$ and $m' = (l, 180^\circ - o)$. The experiments for selecting the number of kernels are shown in the section below in the supplementary material.

B. Analysis on sharp frames

Our approach is based on the observation that there are almost always sharp frames in a blurry video. To verify our observation, we conduct surveys on our real-world video deblurring dataset and two popular datasets: GOPRO by Su et al. [29] and REDS [19] to check the existence of the sharp frames. We compute the variance of image Laplacian of each frame in the videos and find that there exist sharp frames at least for every 20 frames in almost all the videos. We show some samples in Figure 11, and we provide all the figures in the supplementary folders. Furthermore, we demonstrate this observation by showing frames in our datasets. As shown in Fig. 18 and Fig. 19, there is always a nearby sharp frame for the selected blurry frames in the video. These datasets cover almost all the scenarios in our daily lives. Thus, our pipeline is stable and reliable.

C. Results on synthetic data

There are several synthetic datasets for video deblurring [19, 20, 29]. In these datasets, a blurry frame is generated by averaging multiple frames in a sharp video, and the original sharp frame serves as the ground-truth deblurred frame. To compare our method with other baselines, we sample ten videos from GoPro dataset [29]. We adopt PSNR, SSIM, and LPIPS [39] to evaluate the methods. The results are summarized in Table 5.

While our method is not the best in terms of PSNR and SSIM, our method can produce clearer and sharper deblurred results than state-of-the-art methods, as shown in the user study in the main paper. Here, we show more qualitative results on the synthetic dataset in Fig. 12. We also provide two folders of our results on synthetic data. For each image in the folder, the left side is the input, and the right side is our deblurred result.

D. Details of user study

We provide a supplementary description of our user study using the Amazon Mechanical (MTurk) Turk. Pair-wise comparisons are grouped into Human Intelligence Tasks (HITs) that are deployed on the mTurk platform. We construct one HIT for each comparison between our method and a baseline. In each HIT, there are 75 comparisons, of which 70 are “Ours vs. baseline.” The other five comparisons are sentinel comparisons where a ground-truth image from the synthetic dataset is compared to the corresponding blurry image. For each comparison, two images are displayed side-by-side, and the user is asked to pick the sharper and clearer one among the two. The left-right order of each comparison is randomized.

A worker is given 20 minutes to complete a HIT. Each HIT is completed by 30 distinct workers. If a worker gives an incorrect answer on one or more out of the five sentinel comparisons, the answer of this worker is discarded. The compensation for one completed HIT is \$1.2.

E. Grid search for blur kernels

To determine the number of each scale of kernels, we perform a grid search on 10 random sampled synthetic videos from GOPRO dataset [29]. The scales of kernels we choose are 21×21 , 31×31 , 41×41 . And for each scale, we try 2000, 3000, and 4000. The results are summarized in Table 6. According to the results, we select the combination of 4000 blur kernels of size 21×21 , 2000 blur kernels of size 31×31 , and 4000 blur kernels of size 41×41 , which achieve the best L-pips result.

F. More on ablation study

Besides the quantitative experiments in the main paper, we provide more visual comparison here, shown in Figure 9.

G. More on extension

We provide an additional comparison between post-processing by the baseline again and our pipeline. As shown in Figure 10, our pipeline can enhance the result produced by EDVR [34], while applying the baseline again will bring artifact and limited enhancement.

	SSIM	PSNR	LPIPS [39]
Input	0.917	28.11	0.2473
DMPHN [36]	0.927	29.18	0.2041
EDVR [34]	0.945	29.32	0.1926
DeblurGAN-v2 [15]	0.955	30.95	0.1428
Ours	0.930	28.00	0.1618

Table 5: Average results of ten test videos from the GoPro dataset [29]. For PSNR and SSIM, the higher, the better. For LPIPS [40], the lower, the better



Figure 9: The visualization of our ablation study. The result illustrates that using degamma and reweighing improves performance and reduces the artifacts.

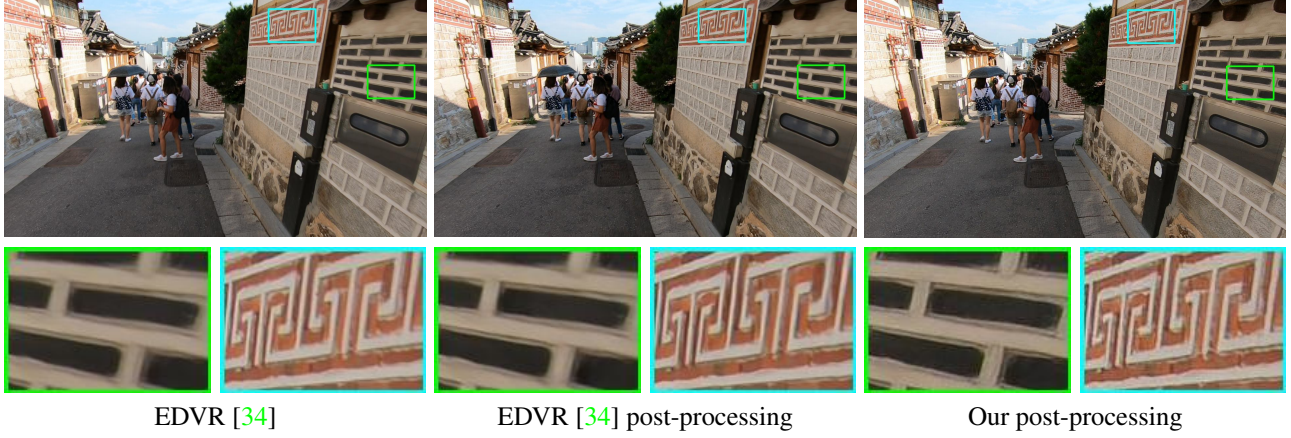


Figure 10: Comparison between post-processing results by EDVR [34] and our pipeline. The result refined by our pipeline is more sharper than the result by applying EDVR [34] again. Applying EDVR [34] again will distort the result.

Number of Kernels	SSIM	PSNR	LPIPS [40]
(2000,2000,2000)	0.923	27.79	0.1537
(2000,2000,3000)	0.921	27.75	0.1548
(2000,2000,4000)	0.922	27.72	0.1574
(2000,3000,2000)	0.924	27.80	0.1537
(2000,3000,3000)	0.923	27.81	0.1539
(2000,3000,4000)	0.924	27.78	0.1540
(2000,4000,2000)	0.923	27.82	0.1582
(2000,4000,3000)	0.923	27.83	0.1578
(2000,4000,4000)	0.924	27.79	0.1545
(3000,2000,2000)	0.923	27.81	0.1548
(3000,2000,3000)	0.922	27.80	0.1565
(3000,2000,4000)	0.923	27.81	0.1541
(3000,3000,2000)	0.924	27.79	0.1532
(3000,3000,3000)	0.924	27.84	0.1543
(3000,3000,4000)	0.924	27.89	0.1560
(3000,4000,2000)	0.922	27.81	0.1538
(3000,4000,3000)	0.924	27.86	0.1550
(3000,4000,4000)	0.922	27.73	0.1543
(4000,2000,2000)	0.922	27.73	0.1572
(4000,2000,3000)	0.923	27.84	0.1542
(4000,2000,4000)	0.924	27.86	0.1516
(4000,3000,2000)	0.925	27.86	0.1519
(4000,3000,3000)	0.923	27.78	0.1535
(4000,3000,4000)	0.923	27.77	0.1522
(4000,4000,2000)	0.924	27.73	0.1545
(4000,4000,3000)	0.923	27.80	0.1547
(4000,4000,4000)	0.924	27.85	0.1560

Table 6: The grid search of the number of blur kernels. The elements in the tuple represent the number of kernels with shape 21×21 , the number of kernels with shape 31×31 , and the number of kernels with shape 41×41 . For PSNR and SSIM, the higher, the better. For LPIPS [39], the lower, the better

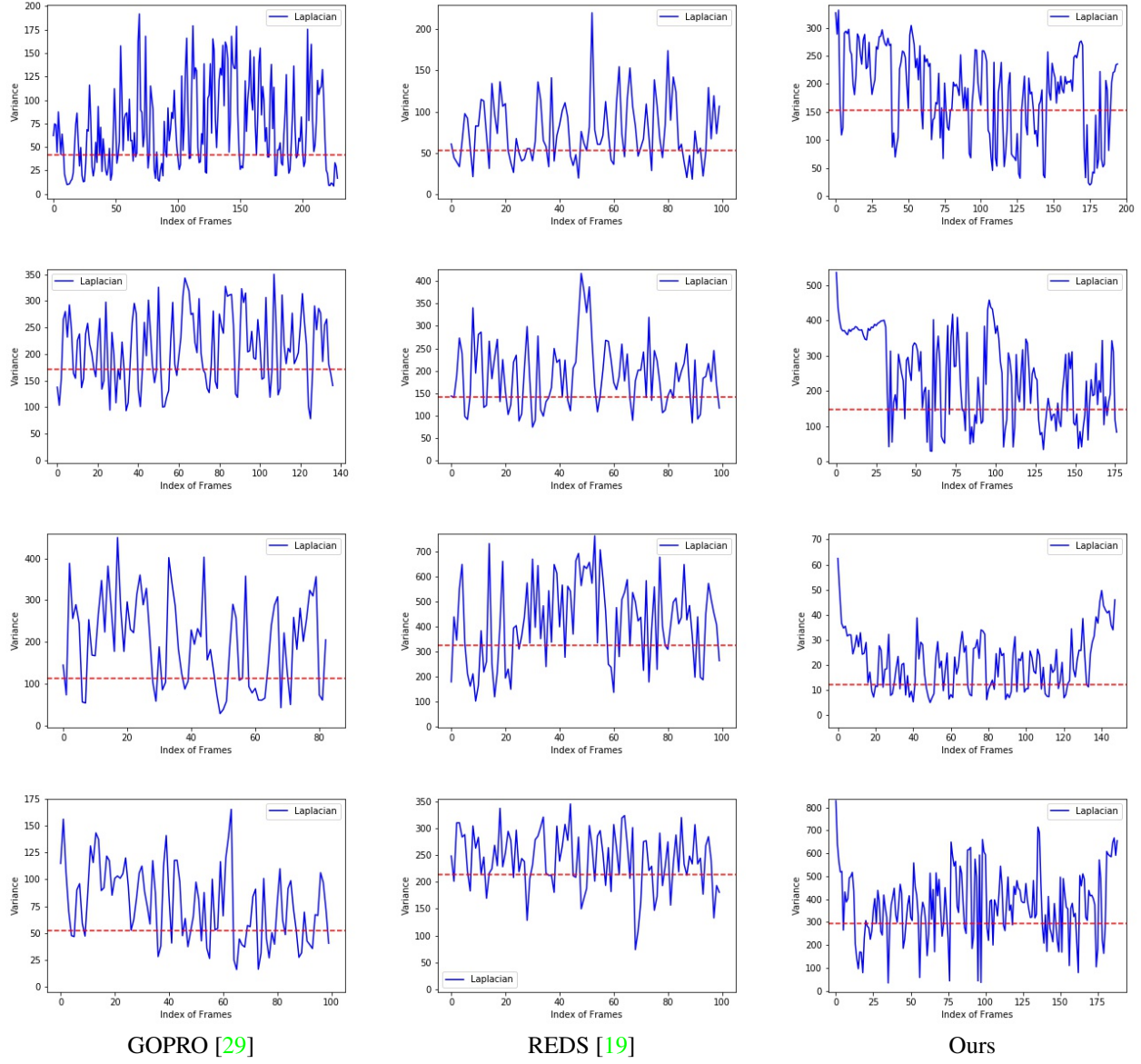


Figure 11: Visualization of the variance of image Laplacian of sampled videos from GOPRO [29], REDS [19] and our dataset. The red dashed line indicates the top 20% value of each video. There exist sharp frames in every 20 frames in all the videos.



Figure 12: More results on examples in the synthetic dataset. Our method recovers high-frequency details, and our result is clearer than the result by DeblurGAN-v2 [15]. PSNR and SSIM disagree with human perception. Zoom in for details.

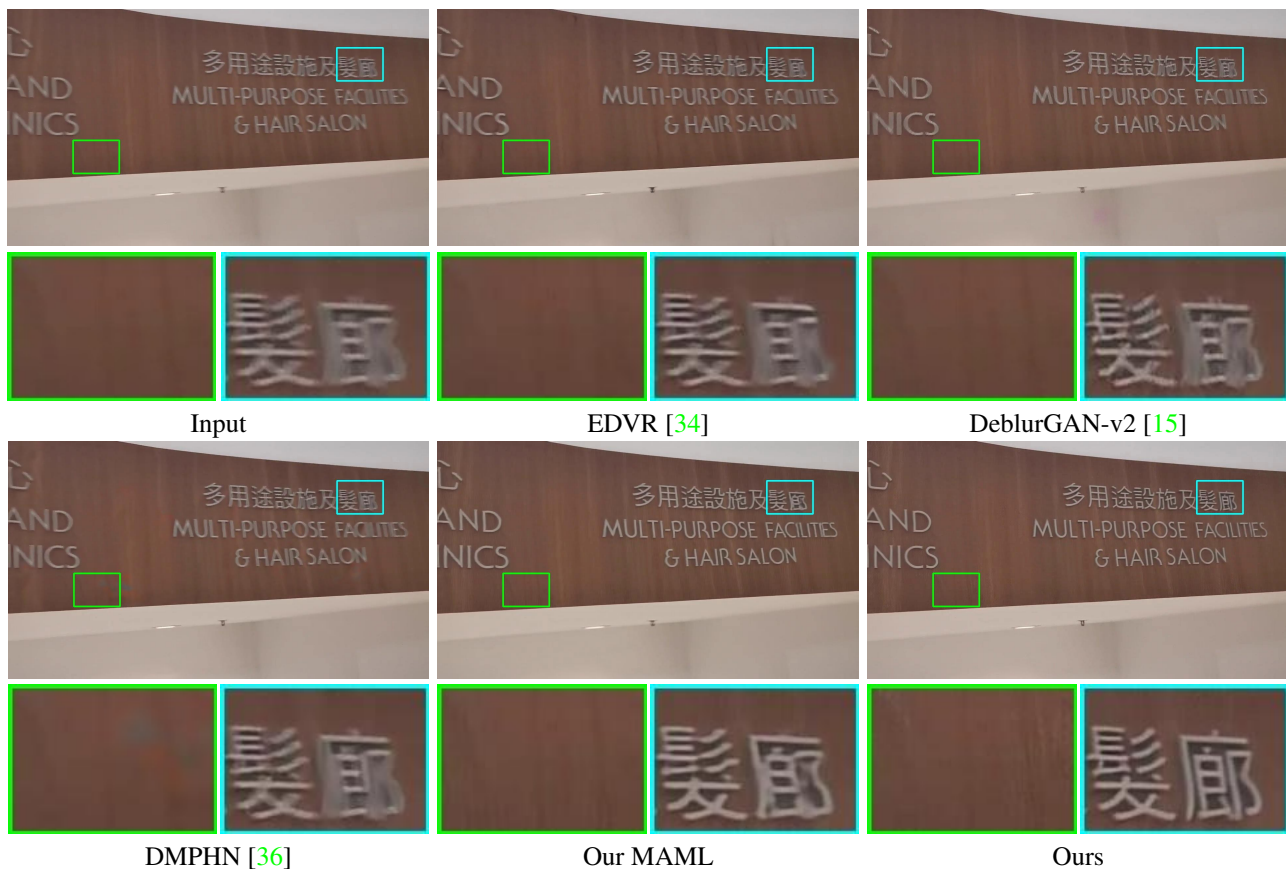


Figure 13: Visual comparisons on our real-world video deblurring dataset. Ours is from our fitting-to-test-data pipeline, and our MAML is from our accelerated pipeline. Our method is capable of restoring the text information.

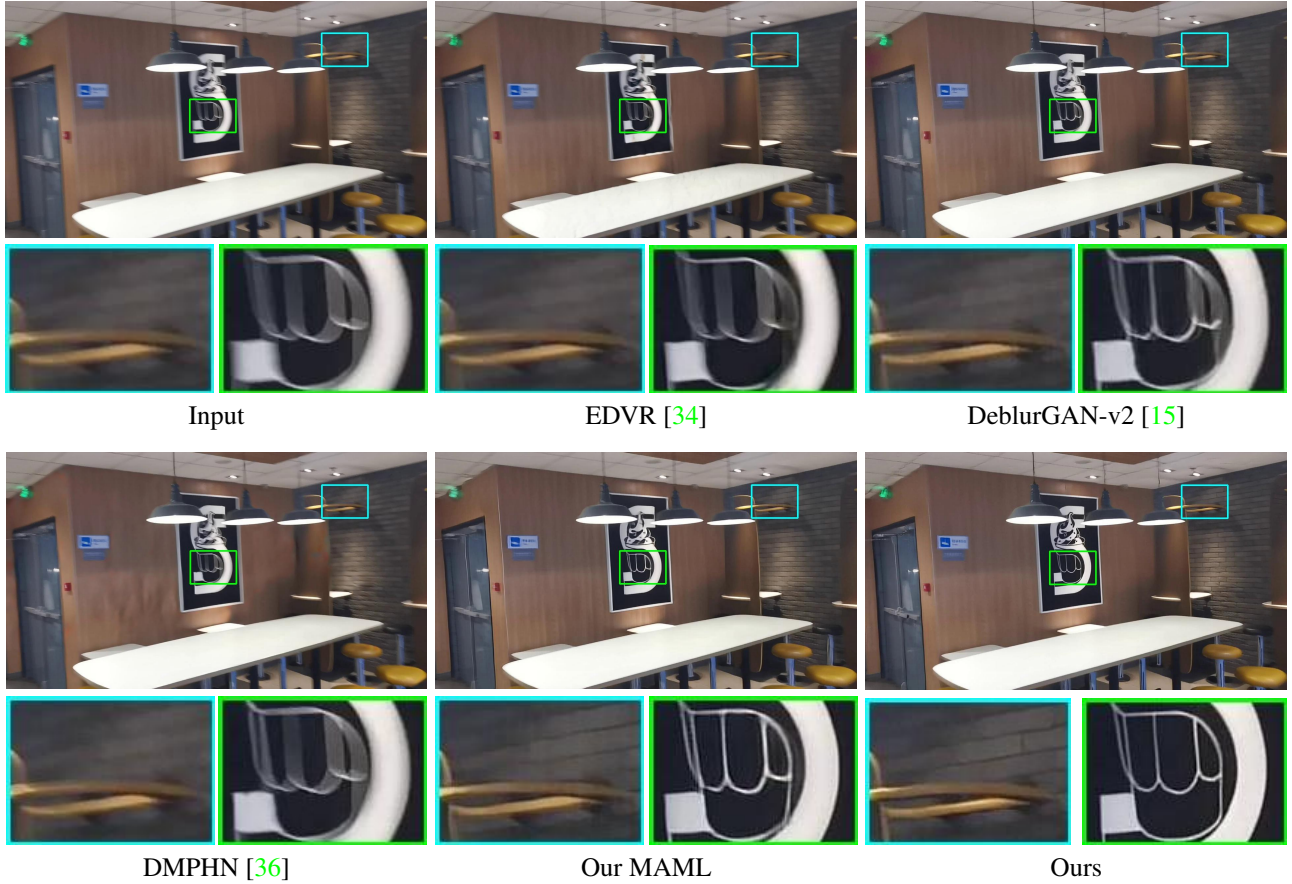


Figure 14: More visual comparisons on our real-world video deblurring dataset. Our method is applicable to both indoor and outdoor scenarios and restores the high-frequency information, i.e., the texture on the wall.

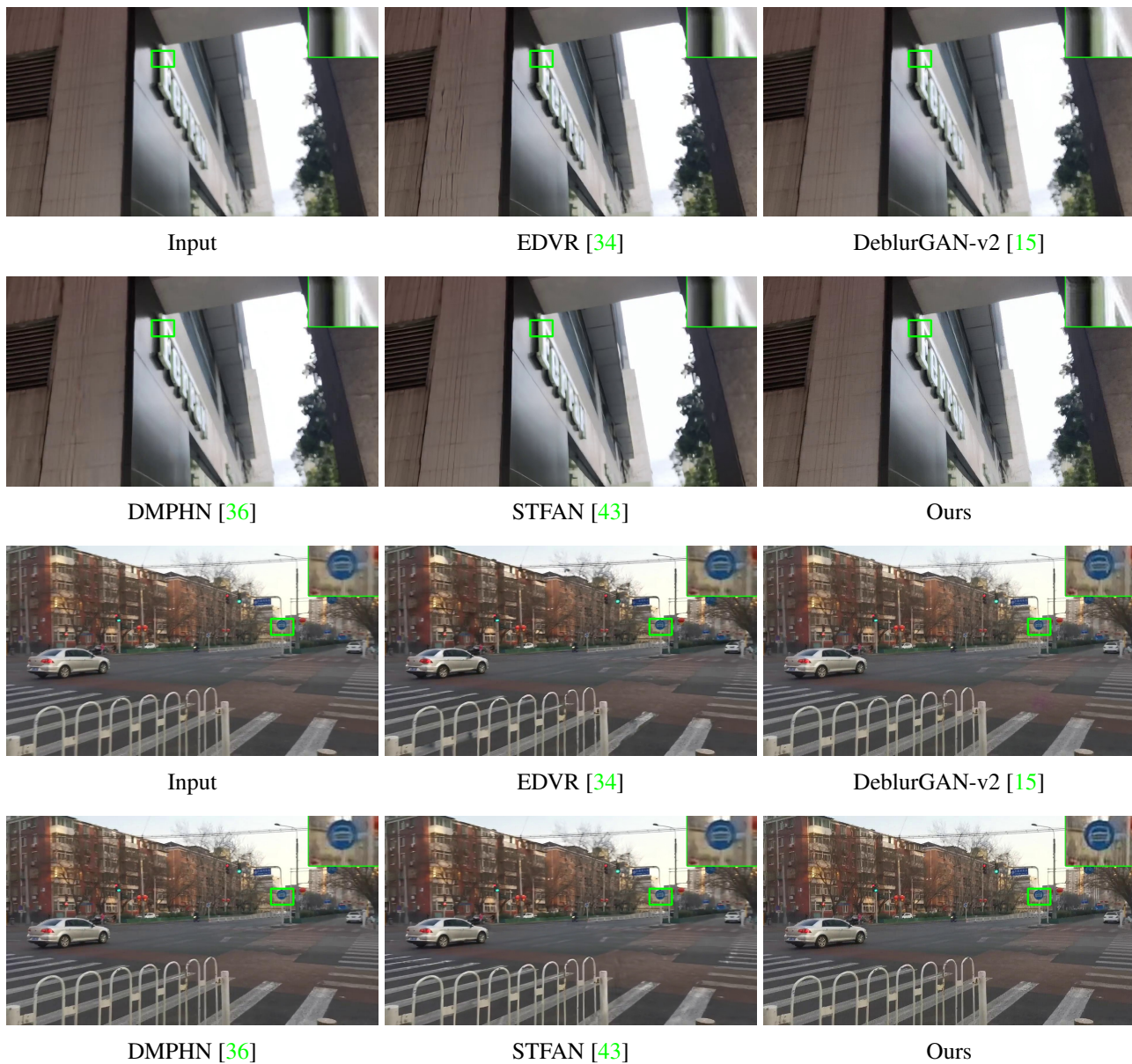


Figure 15: More comparisons on our real-world video deblurring dataset. Zoom in for details.

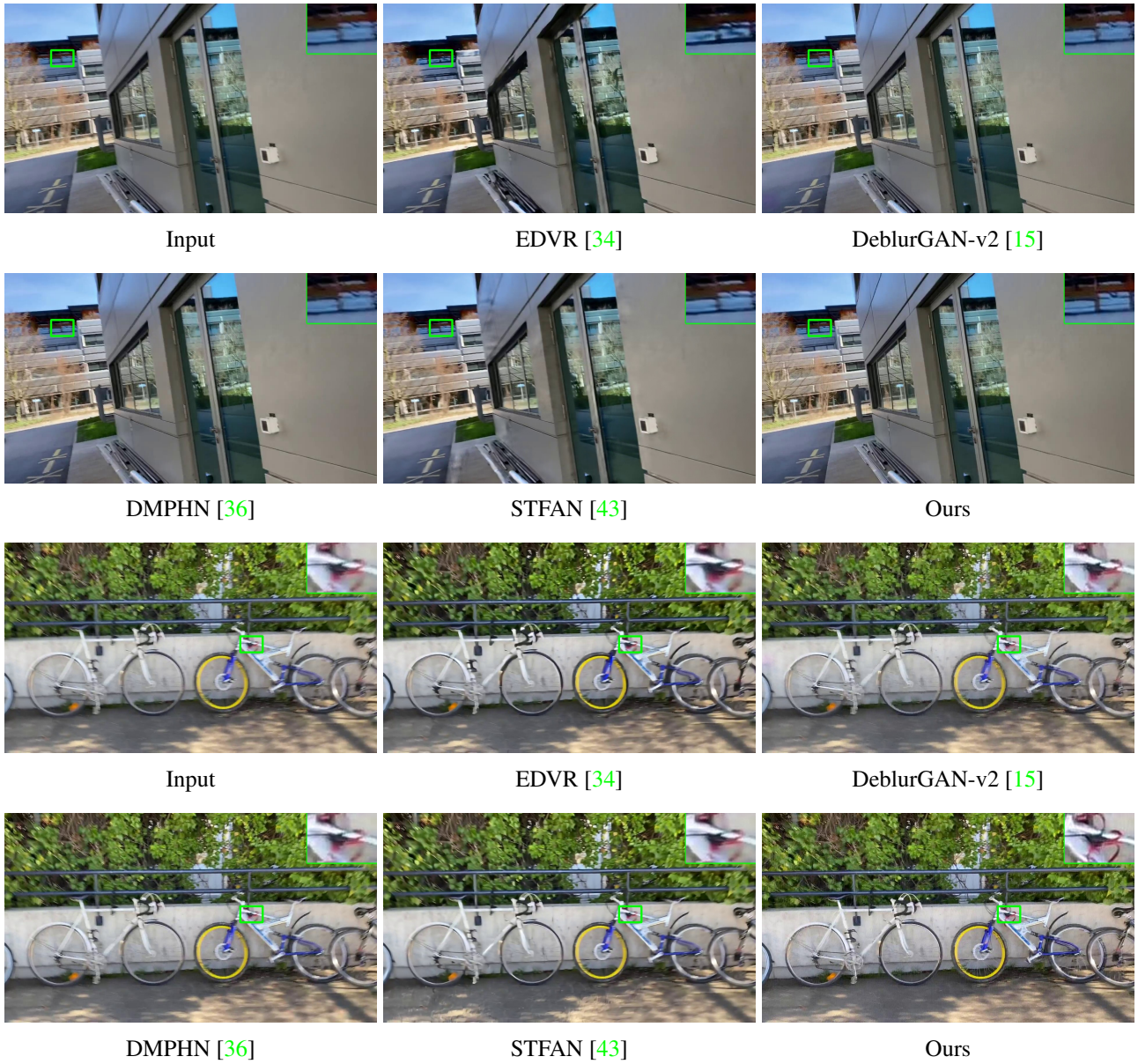


Figure 16: More comparisons on our real-world video deblurring dataset. Zoom in for details.

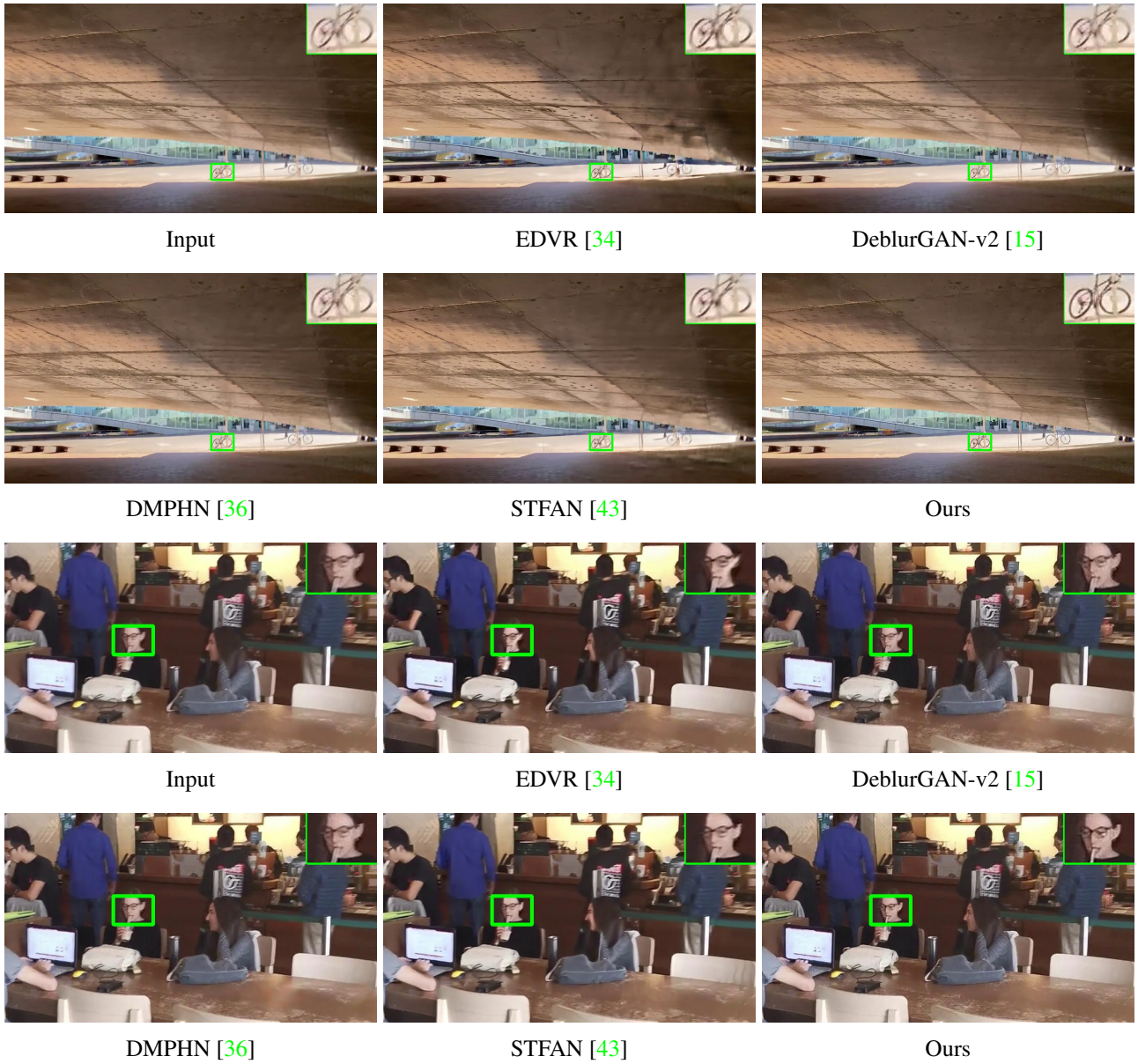
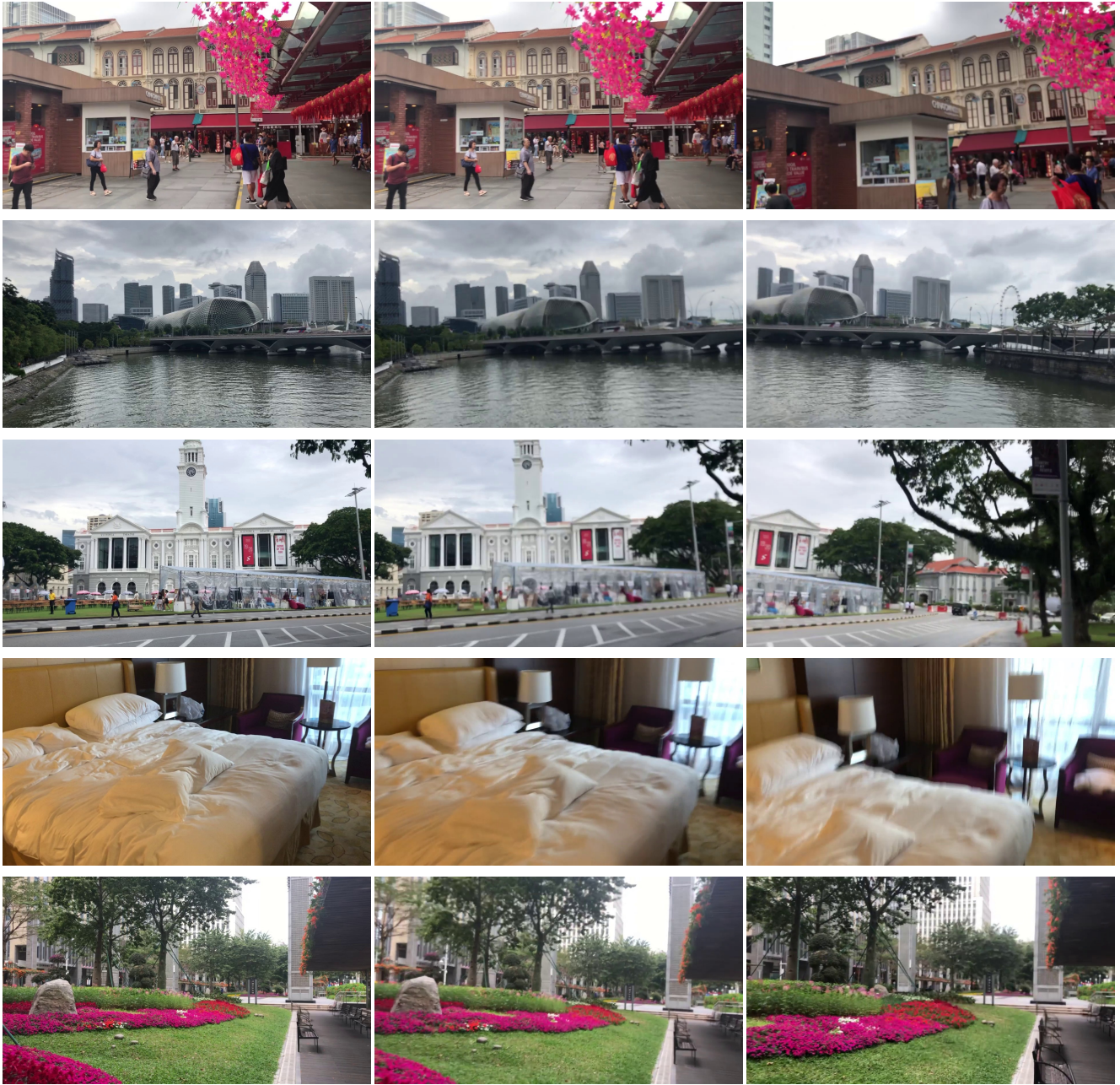


Figure 17: More comparisons on our real-world video deblurring dataset. Zoom in for details.

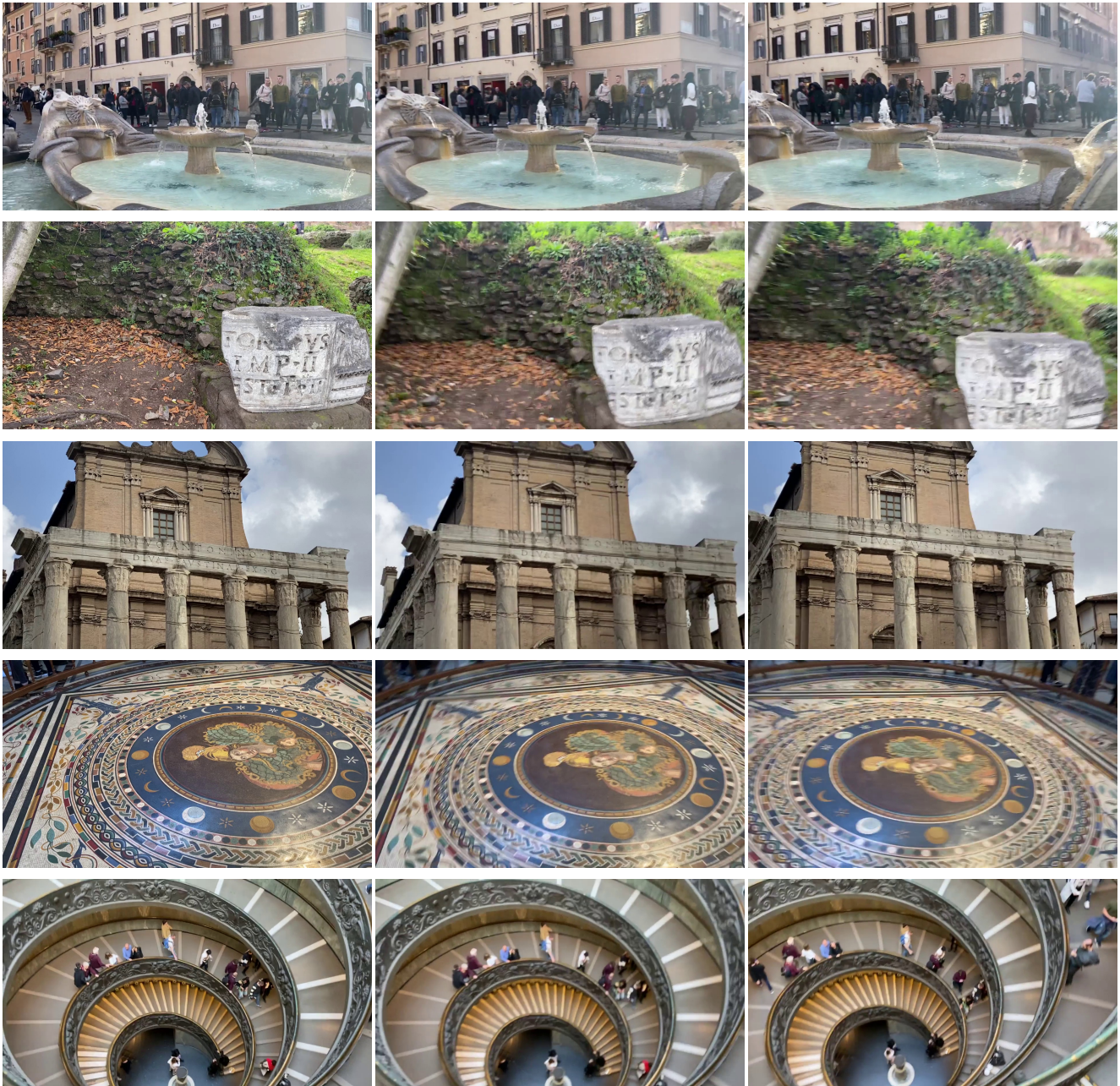


Sharp frame

Blurry frame

Blurry frame

Figure 18: Demonstration on the observation about sharp and blurry frames. For each row, we sample one sharp frame and two blurry frames from each video. Zoom in for details.



Sharp frame

Blurry frame

Blurry frame

Figure 19: More demonstration on the observation about sharp and blurry frames. Zoom in for details.